Preclinical Development of PNT6555, a Boronic Acid–Based, Fibroblast Activation Protein-α (FAP)–Targeted Radiotheranostic for Imaging and Treatment of FAP-Positive Tumors

Sarah E. Poplawski[1], Robin M. Hallett[2], Mark H. Dornan[2], Kyle E. Novakowski[2], Shuang Pan[1], Anthony P. Belanger[3,4], Quang-De Nguyen[3,5], Wengen Wu[1], Albert E. Felten[2], Yuxin Liu[1], Shin Hye Ahn[3,4], Valerie S. Hergott[2], Barry Jones[1], Jack H. Lai[1], Joe A.B. McCann[2], and William W. Bachovchin[1]

[1]*Department of Developmental, Molecular and Chemical Biology, Tufts University Graduate School of Biomedical Sciences, Boston, Massachusetts;* [2]*POINT Biopharma Global Inc., Indianapolis, Indiana;* [3]*Harvard Medical School, Boston, Massachusetts;* [4]*Molecular Cancer Imaging Facility, Dana-Farber Cancer Institute, Boston, Massachusetts; and* [5]*Lurie Family Imaging Center, Dana-Farber Cancer Institute, Boston, Massachusetts*

The overexpression of fibroblast activation protein-α (FAP) in solid cancers relative to levels in normal tissues has led to its recognition as a target for delivering agents directly to tumors. Radiolabeled quinoline-based FAP ligands have established clinical feasibility for tumor imaging, but their therapeutic potential is limited due to suboptimal tumor retention, which has prompted the search for alternative pharmacophores. One such pharmacophore is the boronic acid derivative *N*-(pyridine-4-carbonyl)-D-Ala-boroPro, a potent and selective FAP inhibitor (FAPI). In this study, the diagnostic and therapeutic (theranostic) potential of *N*-(pyridine-4-carbonyl)-D-Ala-boroPro–based metal-chelating DOTA-FAPIs was evaluated. **Methods:** Three DOTA-FAPIs, PNT6555, PNT6952, and PNT6522, were synthesized and characterized with respect to potency and selectivity toward soluble and cell membrane FAP; cellular uptake of the Lu-chelated analogs; biodistribution and pharmacokinetics in mice xenografted with human embryonic kidney cell–derived tumors expressing mouse FAP; the diagnostic potential of ^{68}Ga-chelated DOTA-FAPIs by direct organ assay and small-animal PET; the antitumor activity of ^{177}Lu-, ^{225}Ac-, or ^{161}Tb-chelated analogs using human embryonic kidney cell–derived tumors expressing mouse FAP; and the tumor-selective delivery of ^{177}Lu-chelated DOTA-FAPIs via direct organ assay and SPECT. **Results:** DOTA-FAPIs and their ^{nat}Ga and ^{nat}Lu chelates exhibited potent inhibition of human and mouse sources of FAP and greatly reduced activity toward closely related prolyl endopeptidase and dipeptidyl peptidase 4. ^{68}Ga-PNT6555 and ^{68}Ga-PNT6952 showed rapid renal clearance and continuous accumulation in tumors, resulting in tumor-selective exposure at 60 min after administration. ^{177}Lu-PNT6555 was distinguished from ^{177}Lu-PNT6952 and ^{177}Lu-PNT6522 by significantly higher tumor accumulation over 168 h. In therapeutic studies, all 3 ^{177}Lu-DOTA-FAPIs exhibited significant antitumor activity at well-tolerated doses, with ^{177}Lu-PNT6555 producing the greatest tumor growth delay and animal survival. ^{225}Ac-PNT6555 and ^{161}Tb-PNT6555 were similarly efficacious, producing 80% and 100% survival at optimal doses, respectively. **Conclusion:** PNT6555 has potential for clinical translation as a theranostic agent in FAP-positive cancer.

Key Words: oncology; FAP; radioligand; theranostic; PET

Received Jul. 13, 2023; revision accepted Oct. 17, 2023.

For correspondence or reprints, contact William W. Bachovchin (william.bachovchin@tufts.edu).

Published online Nov. 30, 2023.

J Nucl Med 2024; 65:100–108
DOI: 10.2967/jnumed.123.266345

Fibroblast activation protein-α (FAP, also called seprase) is a member of the dipeptidyl peptidase 4 (DPP4)–like subfamily of serine proteases (*1–3*). FAP is expressed as either a type II integral membrane glycoprotein (*4*) or a soluble plasma protein containing only the extracellular carboxy-terminal catalytic domain (*5*). Relative to normal tissues, FAP is often highly overexpressed in epithelial tumors on the surface of cancer-associated fibroblasts (CAFs) (*6–8*). Less frequently, FAP is overexpressed on neoplastic cells themselves, in certain sarcomas, for example (*8*).

Although FAP is also upregulated in healing wounds and atherosclerotic, arthritic, and fibrotic lesions (*9–13*), it is recognized as a target for the design of anticancer drugs (*14*). There is particular interest in high-affinity, small-molecule catalytic-site ligands that can be linked to a metal chelator such as DOTA for use as theranostic agents: for example, positron-emitting ^{68}Ga for PET or β-emitting ^{177}Lu, ^{161}Tb (which emits Auger electrons and undergoes β-decay (*15*)), or α-emitting ^{225}Ac for radiotherapy (*16*). Unlike FAP, the related postproline cleaving proteases DPP4 and prolyl endopeptidase (PREP) are widely expressed in normal tissues. DPP4 plays a role in glucose metabolism (*17*), whereas the phenotype of PREP-deficient mice suggests that PREP functions in the central nervous system (*18*). High FAP selectivity is, therefore, essential in FAP-targeted radioligands for application in oncology.

A potent and selective inhibitor of FAP (UAMC1110) that is based on the *N*-4-quinolinoyl-Gly-(2*S*)-cyanoPro scaffold, has provided a lead for the development of quinoline FAP inhibitors (FAPIs) (*19–21*). These FAPIs demonstrated the feasibility of FAP radioligands as PET imaging agents in preclinical models and human cancer patients, but therapeutic potential appeared limited by suboptimal tumor retention (*22*), prompting the exploration of alternative FAP ligands. A more recent clinical candidate, FAP-2286, incorporates a cyclic peptide as the FAP-binding moiety, with the aim of harnessing the entropic advantage available from

conformationally restricted cyclic ligands, so as to achieve greater potency and thereby greater tumor retention (*23*). In a mouse model of FAP-positive cancer (FAP-expressing human embryonic kidney [HEK] cells), ^{177}Lu-FAP-2286 did achieve greater tumor retention and treatment responses than ^{177}Lu-FAPI-46, the leading quinoline derivative (*24*).

A different approach can be based on the boronic acid derivative *N*-(pyridine-4-carbonyl)-D-Ala-boroPro (3099), first discovered and characterized by Poplawski et al. (*25*). The nanomolar potency of 3099 and the high selectivity for FAP over other DPP4-like subfamily enzymes provides the rationale for its investigation as a FAP-targeting moiety. In this study, the feasibility of amino-terminally blocked D-Ala-boroPro as a FAP-targeting element in theranostic radioligands was investigated, with a focus on PNT6555, PNT6952, and PNT6522 (Fig. 1)—in which the DOTA chelator was N-terminally linked to D-alanine by either an aminobenzoic acid residue (PNT6555), a tranexamic acid residue (PNT6952), or a Gly-Gly-Val tripeptide (PNT6522).

MATERIALS AND METHODS

A complete version of Materials and Methods, including details of instrumentation, radiochemistry, in vivo imaging protocols, reagents, reaction buffers, and vendors, is provided in the supplemental materials (supplemental materials are available at http://jnm.snmjournals.org).

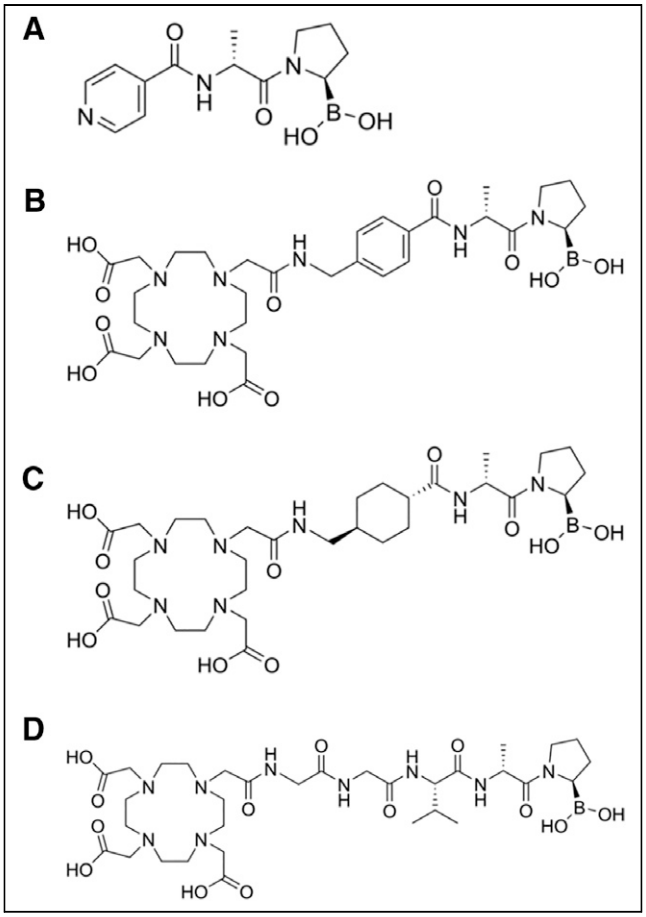

FIGURE 1. Structures of FAP ligands. (A) *N*-(pyridine-4-carbonyl)-D-Ala-boroPro (3099). (B) DOTA-AmBz-D-Ala-boroPro (AmBz: aminomethylbenzoyl) (PNT6555). (C) DOTA-TXA-D-Ala-boroPro (TXA: transexamic acid) (PNT6952). (D) DOTA-Gly-Gly-Val-D-Ala-boroPro (PNT6522).

In Vivo Procedures

The protocol for the tumor model involving HEK cell–derived tumors expressing mouse FAP (HEK-mFAP) was approved by the Dana-Farber Cancer Institute (Boston, Massachusetts) Institutional Animal Care and Use Committee. Mouse serum was collected by cardiac puncture using a protocol approved by the Tufts University Institutional Animal Care and Use Committee.

Synthesis of FAP Ligand Precursors

PNT6555, PNT6522, and PNT6952 were synthesized as previously described by Bachovchin et al. (*26*).

Radiochemistry of ^{68}Ga-, ^{177}Lu-, ^{225}Ac-, and ^{161}Tb-Chelated Compounds

Radioligands were prepared by heating precursors with $^{177}LuCl_3$, $^{68}GaCl_3$, $^{225}Ac(NO_3)_3$, or $^{161}TbCl_3$. Radiochemical identities were confirmed by chromatography.

HEK-mFAP and HEK-Mock Cell Lines

HEK-mFAP and HEK cells transfected with empty vector (HEK-Mock) (*27*) were propagated in standard culture medium with the addition of G418 (Geneticin; Thermo Fisher Scientific) to sustain stable transgene expression.

In Vitro Fluorometric IC_{50} Measurements

Half-maximal inhibitory concentration (IC_{50}) values of FAP ligands for recombinant human FAP, DPP4, and PREP were determined. FAP (pH 7.5), PREP (pH 7.5), and DPP4 (pH 8.0) were incubated at room temperature for 10 min with 1:10 serial dilutions of FAP ligands (PNT6555, PNT6952, and PNT6522) in 96-well plates. 7-Amino-4-methylcoumarin (AMC) fluorogenic substrates (carboxybenzyl (*Z*)-Gly-Pro-AMC for FAP and PREP and Gly-Pro-AMC for DPP4) were added to the reactions at a final concentration of 25 μM. After further incubation for 15 min at room temperature, enzyme activity was measured by fluorimetry ($Ex_{380\ nm}$:$Em_{460\ nm}$). A modified method with *N*-(4-quinolinoyl)-D-Ala-Pro (3144)–AMC as the FAP substrate was also used for IC_{50} assays with recombinant human and mouse FAP. The enzymes were incubated at 37°C for 10 min with 1:10 serial dilutions of FAP ligands. 3144-AMC was added at a final concentration of 25 μM, and incubation was continued for a further 30 min at 37°C before fluorimetry.

For IC_{50} assays with serum samples, 1:10 dilutions of human serum and Sprague–Dawley rat serum and a 1:100 dilution of mouse serum were incubated at 37°C for 10 min with 1:10 serial dilutions of FAP ligands. 3144-AMC was added at a final concentration of 25 μM (rat serum) or 50 μM (human serum and mouse serum), and incubation was continued for a further 30 min at 37°C before fluorimetry.

For IC_{50} assays with cell membrane FAP, HEK-mFAP cells were harvested from bulk cultures grown to approximately 80% confluency and plated in 96-well plates. After incubation overnight, 1:10 serial dilutions of FAP ligands were incubated with the cells for 1 h. 3144-AMC was added at a final concentration of 20 μM, and 37°C incubation was continued for a further 30 min before fluorimetry.

ICP-MS Assay for In Vitro Uptake and Internalization of ^{nat}Lu-Chelated FAP Ligands

In vitro cellular uptake of ^{nat}Lu-FAP ligands was investigated by inductively coupled plasma mass spectrometry (ICP-MS) analysis of total ^{nat}Lu associated with HEK-mFAP or HEK-Mock cells. The internalized fraction represented the ^{nat}Lu remaining after an acid wash to remove any cell membrane–bound inhibitor. HEK-mFAP or HEK-Mock cells were seeded in 6-well plates (Costar) at 4×10^6 cells/2 mL/well in serum-free RPMI 1640 assay medium and incubated (37°C, 5% CO_2) for 18–24 h. Medium was aspirated and replaced with 1, 5, 10, or 100 nM ^{nat}Lu-PNT6555 for the measurement of FAP ligand uptake or with 10 nM ^{nat}Lu-PNT6555, ^{nat}Lu-PNT6952, or

^{nat}Lu-PNT6522 for the measurement of FAP ligand uptake and internalization. After incubation for 1 h at 37°C, the cells were washed twice with 1 mL of ice-cold phosphate-buffered saline (PBS). For the measurement of total cellular FAP ligand uptake ($^{nat}Lu_{total}$), the cells were lysed by incubation at room temperature in 0.3 M NaOH for 5 min, after which the samples were passed through a 23-gauge needle to shear DNA. For the measurement of cellular internalization, 1 mL of ice-cold 50 mM glycine–100 mM NaCl (pH 2.8) buffer was added to the cells after the PBS wash step described before. After incubation at 4°C for 10 min, the cells were washed twice with 1 mL of ice-cold PBS and then lysed as described before to provide samples for the measurement of internalized FAP ligand ($^{nat}Lu_{internal}$). The protein concentrations of the total uptake and internalization samples were measured by the Bradford assay (Bio-Rad). Postlysis samples (300 μL) were microwave digested with 0.5 mL of ultrapure water and 2.0 mL of ultra–high-purity nitric acid. The samples were further diluted with ultrapure water to achieve 2.8% nitric acid. An internal standard (final concentration of indium of 5 ppb) was added to the samples, and indium at 0.1 ppt was added to 500-ppt Lu standards for the creation of a standard curve. ICP-MS was conducted in low-resolution mode. Calibrant intensities were normalized to the intensities of the internal controls, and the intensities in blank samples were subtracted to create linear calibration curves. The total cellular uptake of ^{nat}Lu after incubation of HEK-mFAP cells with 1, 5, 10, or 100 nM ^{nat}Lu-PNT6555 was expressed as the absolute amount (nanograms). The percentage internalization of ^{nat}Lu was calculated as ($^{nat}Lu_{internal}$/$^{nat}Lu_{total}$) × 100.

HEK-mFAP Mouse Tumor Xenograft Model

Six-week-old male Fox Chase mice with severe combined immunodeficiency were injected subcutaneously with HEK-mFAP cells. Tumor growth was determined by measurement of tumor width (W) and length (L) with calipers, and tumor volume (V) expressed in mm^3 was calculated by the formula $V = (W_2 \times 0.5L)$.

Formulation and In Vivo Administration of Radioligands

Radioligands diluted in PBS were administered to anesthetized mice by a single injection into the lateral tail vein.

Biodistribution of ^{68}Ga- and ^{177}Lu-Radioligands In Vivo

HEK-mFAP tumor–bearing mice were injected intravenously with defined doses of ^{68}Ga-PNT6555 or ^{177}Lu-radioligands. At designated time points, blood and tissues were collected from 3 mice per treatment and counted for radioactivity. Tissue weights were measured for determination of the percentage injected dose per gram (%ID/g).

PET and SPECT

After intravenous injection of radioligands, ^{68}Ga imaging by small-animal PET/CT and ^{177}Lu SPECT imaging were performed.

Antitumor Activity of ^{177}Lu-, ^{225}Ac-, and ^{161}Tb-Radioligands In Vivo

Mice bearing HEK-mFAP tumors of the volumes specified in the Results section were administered ^{177}Lu-, ^{225}Ac-, or ^{161}Tb-radioligands, vehicle, or precursor ligands (6 mice per group) on day 1. Health checks were performed, and body weights and tumor dimensions were measured weekly. Mortality or euthanasia was used interchangeably for plotting mouse survival curves. Tumor growth curves were plotted up to the time of the earliest incidence of a mortality/euthanasia endpoint in each of the control and test groups.

Statistical Analysis

In vitro and in vivo data were analyzed using Prism 6 (GraphPad Software), and results are presented as mean ± SEM.

RESULTS

Potency and Selectivity of FAP Inhibitors for Human Recombinant FAP

PNT6555, PNT6952, and PNT6522 when not chelated with metals exhibited low nanomolar IC_{50} values for FAP that were ~200- to ~1000-fold and ~10,000- to ~30,000-fold less, respectively, than the values for PREP and DPP4 (Table 1). The introduction of the metals reduced potency toward FAP by 2- to 48-fold, depending on the compound (Table 1). Metal chelation also reduced affinity for PREP by ≤4-fold. No inhibition of DPP4 was detectable.

Potency of FAP Inhibitors for Biologically Relevant Forms of FAP

The potencies of nonchelated and metal-chelated compound were evaluated toward human and rodent serum FAP, and mouse cell surface FAP in HEK-mFAP cells. The 3144-AMC substrate

TABLE 1
Selective Inhibition of FAP by Precursor and Nonradioactive Lu/Ga-Chelated PNT6555, PNT6952, and PNT6522 In Vitro

	Recombinant human enzyme IC_{50} (nM)*			Selectivity index†	
Compound	FAP	PREP	DPP4	PREP	DPP4
PNT6555	3.9 ± 0.3	900 ± 97	>100,000	230	>26,000
^{177}Lu-PNT6555	16 ± 3.0	4,100 ± 740	>100,000	260	>6,300
^{68}Ga-PNT6555	55 ± 3.0	3,600 ± 510	>100,000	65	>1,800
PNT6952	4.7 ± 0.2	4,700 ± 780	>100,000	1,000	>21,000
^{177}Lu-PNT6952	13 ± 1.2	34,000 ± 10,000	>100,000	2,500	>7,400
^{68}Ga-PNT6952	84 ± 5.3	>10,000	>10,000	>120	>120
PNT6522	12 ± 0.6	9,200 ± 2,000	>100,000	760	>8,300
^{177}Lu-PNT6522	25 ± 2.0	10,000 ± 3,700	>100,000	390	>3,900
^{68}Ga-PNT6522	570 ± 95	37,000 ± 12,000	>100,000	65	>160

*IC_{50} values obtained in fluorometric assays with *Z*-Gly-Pro-AMC (FAP and PREP) and Gly-Pro-AMC (DPP4) substrates are expressed as mean (n = 3) ± SEM.

†Calculated as IC_{50} (PREP)/IC_{50} (FAP) and IC_{50} (DPP4)/IC_{50} (FAP).

TABLE 2
Potency of Inhibition of Soluble Recombinant, Cell Membrane, and Serum Forms of Human and Rodent FAP by Precursor and Nonradioactive Lu/Ga-Chelated PNT6555, PNT6952, and PNT6522 In Vitro

Compound	Recombinant soluble FAP IC_{50} (nM)		HEK-mFAP IC_{50} (nM): mouse	Serum IC_{50} (nM)		
	Human	Mouse		Human	Mouse	Rat
PNT6555	1.8 ± 0.4	0.2 ± 0.01	0.8 ± 0.03	2.5 ± 0.4	0.2 ± 0.01	0.3 ± 0.01
^{177}Lu-PNT6555	6.6 ± 0.5	0.4 ± 0.01	1.2 ± 0.1	10 ± 1.7	0.2 ± 0.02	0.4 ± 0.1
^{68}Ga-PNT6555	98 ± 5.4	17 ± 0.9	47 ± 5.9	100 ± 9.3	16 ± 1.6	24 ± 6.4
PNT6952	0.5 ± 0.1	0.3 ± 0.003	1.2 ± 0.1	1.3 ± 0.3	0.3 ± 0.03	0.3 ± 0.01
^{177}Lu-PNT6952	4.7 ± 0.5	1.6 ± 0.1	6.8 ± 0.6	8.0 ± 2.0	1.9 ± 0.1	1.8 ± 0.1
^{68}Ga-PNT6952	47 ± 6.0	11 ± 1.0	22 ± 1.3	42 ± 5.5	13 ± 0.6	14 ± 2.0
PNT6522	1.9 ± 0.4	0.5 ± 0.1	1.7 ± 0.4	1.4 ± 0.2	0.5 ± 0.04	0.5 ± 0.01
^{177}Lu-PNT6522	4.7 ± 0.3	2.3 ± 0.2	12 ± 0.5	11 ± 2.0	2.5 ± 0.1	3.3 ± 0.1
^{68}Ga-PNT6522	140 ± 30	87 ± 18	82 ± 3.1	190 ± 32	83 ± 7.4	64 ± 5

IC_{50} values obtained in 3144-AMC fluorometric assays are expressed as mean (n = 3) ± SEM.

(Supplemental Fig. 1) (*28*) was used to specifically measure FAP activity in the unfractionated biologic matrices, and as a benchmark for the inhibition of FAP in biologic samples; FAP inhibitor potency toward soluble recombinant FAP was also evaluated with this substrate. When not chelated to metals, the compounds exhibited subnanomolar to low-nanomolar IC_{50} values in assays with all sources of FAP (Table 2). Lu-chelation reduced the potency to a smaller extent than Ga-chelation in both the Z-Gly-Pro-AMC and 3144-AMC assays, and with both soluble and cell membrane forms of FAP (Tables 1 and 2).

Cellular Uptake and Internalization of FAP Inhibitors

The FAP dependence of the cellular uptake of ^{nat}Lu-PNT6555 was investigated by comparing the total uptake in HEK-mFAP versus HEK-Mock cells. Measurement of total cell-associated ^{nat}Lu-PNT6555 by ICP-MS demonstrated that uptake required the expression of FAP (Fig. 2A). ICP-MS measurements of the total cell bound and internalized amounts of ^{nat}Lu in HEK-mFAP cells after 1 h incubation with ^{nat}Lu-PNT6555, ^{nat}Lu-PNT6952 or ^{nat}Lu-PNT6522 indicated that ^{nat}Lu-PNT6555 exhibited the greatest degree of internalization (Fig. 2B).

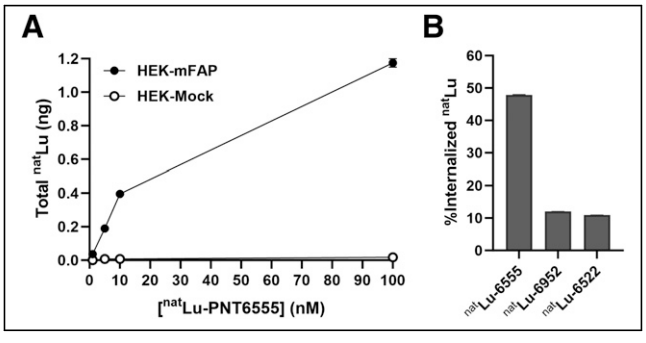

FIGURE 2. Cellular uptake and internalization of ^{nat}Lu-chelated FAP ligands. (A) Total ^{nat}Lu uptake by HEK-mFAP and HEK-Mock cells after 1 h of incubation at 37°C with increasing concentrations of ^{nat}Lu-PNT6555 in vitro. (B) Comparison of internalized fractions of ^{nat}Lu after 1 h of incubation of HEK-mFAP cells with 10 nM ^{nat}Lu-PNT6555, ^{nat}Lu-PNT6952, or ^{nat}Lu-PNT6522 in vitro.

Biodistribution of Radiolabeled FAP Inhibitors in Tumor-Bearing Mice

^{68}Ga-PNT6555 and ^{68}Ga-PNT6952 exhibited selective uptake into HEK-mFAP tumors (Fig. 3A). Small-animal PET indicated that the radioligands rapidly entered the tumors, and while they were progressively cleared from the blood and normal tissues via the kidneys and the bladder, tumor activity increased rapidly over the first 5 min after injection, and more slowly but continuously thereafter (Fig. 3C; Supplemental Fig. 2). Elimination from blood, liver, and muscle resulted in radioligand levels that were distinctly lower in normal tissues than in tumors by ~25 min after administration (Fig. 3C), and high-contrast PET images of tumors were obtained at 60 min (Fig. 3C). All 3 ^{177}Lu-FAP radioligands exhibited selective uptake in tumors 4 h after a single dose in HEK-mFAP tumor–bearing mice (Fig. 4A; Supplemental Fig. 3). Intratumoral levels of all 3 radioligands decreased between 4 and 48 h, but high tumor-to-normal tissue ratios were maintained from 48 to 168 h. Analysis of the area under the curve (AUC) ((%ID/g)·h) for the period from 4 to 168 h indicated that the accumulation of ^{177}Lu-PNT6555 in the tumor was significantly greater than that for ^{177}Lu-PNT6952 or ^{177}Lu-PNT6522 ($P < 0.0001$) (Table 3; Supplemental Table 1), but the increase in ^{177}Lu-PNT6555 between 48 and 168 h was not statistically significant. Although the limited uptake in normal tissues exhibited some variation between the 3 radioligands (Table 3), these differences were not statistically significant (Supplemental Table 1). The highest levels of uptake into normal tissues occurred in kidney, liver, bone and skin for ^{177}Lu-PNT6555, kidney for ^{177}Lu-PNT6952, and kidney and bone for ^{177}Lu-PNT6522 (Table 3; Supplemental Fig. 3). However, the high initial tumor uptake and kinetics of tumor retention resulted in tumor-to-normal tissue AUC ratios of 15 to 19 in these tissues (Table 3). This is illustrated by the pharmacokinetic profiles in tumor and kidney (Fig. 4A), and the retention of ^{177}Lu-PNT6555 in the tumors was apparent in SPECT images collected from 3 to 120 h (Fig. 4B).

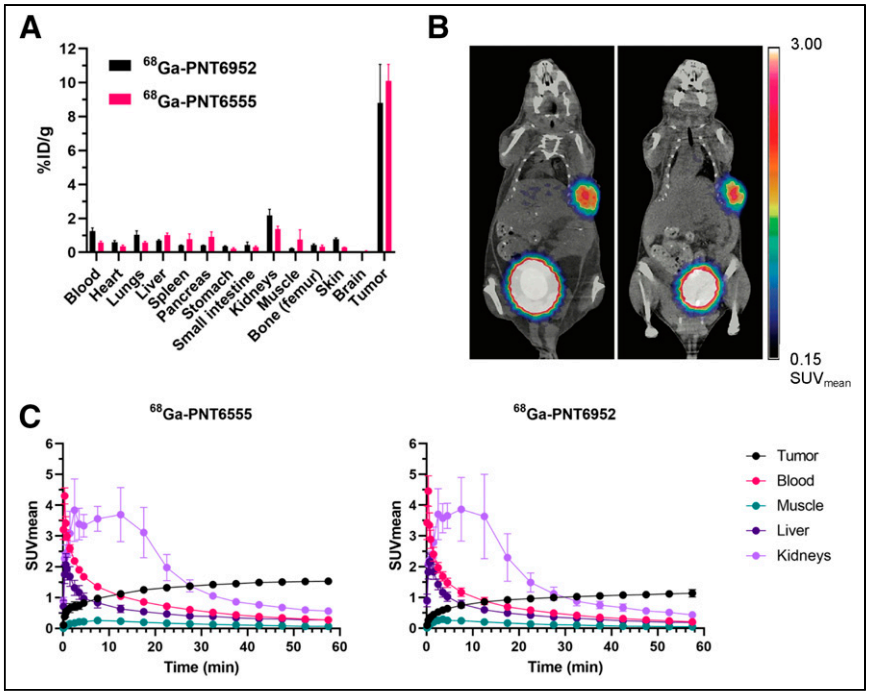

FIGURE 3. Biodistribution, pharmacokinetics, and PET imaging for ^{68}Ga-PNT6555 and ^{68}Ga-PNT6952 in mice bearing ~300-mm^3 HEK-mFAP tumors administered doses of 8–10 MBq. (A) Biodistribution of radioligands 60 min after injection. Mean ± SEM %ID/g values are shown for 3 animals per tissue. (B) Biodistribution of radioligands determined by PET imaging 60 min after administration in representative animals from groups of 3. (C) Time–activity curves for tissue uptake of radioligands determined by PET imaging. SUV_{mean} ± SEM are shown for 3 animals per tissue.

Antitumor Activity of PNT6555, PNT6952, and PNT6522 ^{177}Lu-Radioligands

^{177}Lu-PNT6555, ^{177}Lu-PNT6952, and ^{177}Lu-PNT6522 were administered to HEK-mFAP tumor–bearing mice as a single dose of 15, 30, or 60 MBq. These doses were selected to enable efficacy to be directly compared with ^{177}Lu-FAPI-46 and ^{177}Lu-FAP-2286, previously evaluated in a HEK-FAP tumor model (*24*). ^{177}Lu-radioligands produced dose-dependent delays in tumor growth, whereas no discernable effect was produced by unlabeled precursors (Fig. 5A). On the last day of tumor measurement before mortality in control groups, tumor growth was significantly inhibited at all doses investigated (Supplemental Fig. 4A). ^{177}Lu-PNT6555 produced the longest tumor growth delay (Fig. 5A), with the rank order of efficacy being ^{177}Lu-PNT6555 > ^{177}Lu-PNT6952 > ^{177}Lu-PNT6522. The same rank order was also reflected in animal survival (Fig. 5B). The radioligands appeared to be well tolerated, and weight loss was ≤10% and transient (Supplemental Fig. 5).

Antitumor Activity of ^{225}Ac-PNT6555 and ^{161}Tb-PNT6555

To HEK-mFAP tumor–bearing mice, ^{225}Ac-PNT6555 was administered as a single dose of 5, 25, or 50 kBq, and ^{161}Tb-PNT6555, as a single dose of 15, 30, or 60 MBq. ^{225}Ac-PNT6555 doses were based on single doses of ^{225}Ac-FAPI-46 that were safe and effective in the PANC-1 xenograft model (*29*), and ^{161}Tb-PNT6555 doses, on safe and effective single doses of radiometal targeted to L1 cell adhesion protein or folate receptor (*30*,*31*). Both ^{225}Ac-PNT6555 and ^{161}Tb-PNT6555 produced dose-dependent delays in tumor growth at all dose levels (Fig. 6A), and before mortality of control animals, tumor volumes were significantly reduced (Supplemental Fig. 4B). Mean tumor volume in mice that received nonradiolabeled PNT6555 appeared to be increased above that in vehicle-treated mice in the ^{225}Ac-PNT6555 experiment. Although this effect was statistically significant, it was not pharmacologically meaningful because it was small and not seen in the ^{177}Lu-PNT6555 (Fig. 5A) and ^{161}Tb-PNT6555 experiments (Fig. 6A). ^{225}Ac-PNT6555 and ^{161}Tb-PNT6555 increased animal survival in a dose-dependent manner (Fig. 6B). Both radioligands were well tolerated, as indicated by minimal effect on body weight (Supplemental Fig. 6).

DISCUSSION

The selective inhibition of FAP over the dipeptidyl peptidases and PREP by 3099, which was achieved by the pyridin-4-carbonyl blocking group at the N terminus, and D-alanine at P_2, respectively (*25*), was maintained in PNT6555, PNT6952, and PNT6522. When expressed as a cell membrane protein in HEK-mFAP cells, the catalytic site of FAP was found to be pharmacologically accessible to the D-AlaboroPro–based ligands and to be essential for the cellular uptake of ^{nat}Lu-PNT6555 by HEK-mFAP cells. In vivo, ^{68}Ga-PNT6555 and ^{68}Ga-PNT6952 were selectively retained in HEK-mFAP tumors, resulting in PET images with high tumor-to-background contrast. The biodistribution of ^{177}Lu-PNT6555, ^{177}Lu-PNT6952, and ^{177}Lu-PNT6522 in HEK-mFAP tumor–bearing mice confirmed the selective targeting of the HEK-mFAP tumors and revealed that ^{177}Lu-PNT6555 exhibited the greatest tumor accumulation, consistent with its greater cellular internalization compared with ^{nat}Lu-PNT6952 and ^{nat}Lu-PNT6522 in vitro.

The premise for development of FAP-targeted radioligands is that the tumor-to-normal tissue ratios of FAP activity in human cancer will be sufficient to ensure pharmacologic effects on the tumor while avoiding damage to normal cells and tissues. However, most mouse tumor models fail to mimic the tumor to normal tissue FAP ratios found in humans, with mouse models having both lower levels of FAP in the tumor and higher levels in the blood than humans (*28*) (S.E. Poplawski, PhD, unpublished data, 2011). Nonetheless, an albumin binding FAP-radioligand, ^{177}Lu-FAP6-IP-DOTA, produced significant tumor responses in mice implanted with multiple tumor cell lines that were not engineered to overexpress FAP, and tumor targeting therefore relied on the FAP expressed in the tumor stroma (*32*). However, the levels of responsiveness to ^{177}Lu-FAP6-IP-DOTA across the KB, HT29, U87MG, and 4T1 tumor models investigated did not correlate with ex vivo staining intensity of stromal FAP for reasons that are not well understood (*32*). In comparison to these models, the HEK-mFAP tumor model is artificial and potentially somewhat problematic because the FAP-levels in the tumor are substantially greater than found in most human cancers, and the FAP is expressed on the neoplastic cells rather than on the stromal CAFs, as in human epithelial cancers. Because of the latter, the FAP targeting is directed at the cancer cells rather than the CAFs, as it would be in humans, and it is unclear how this might affect the

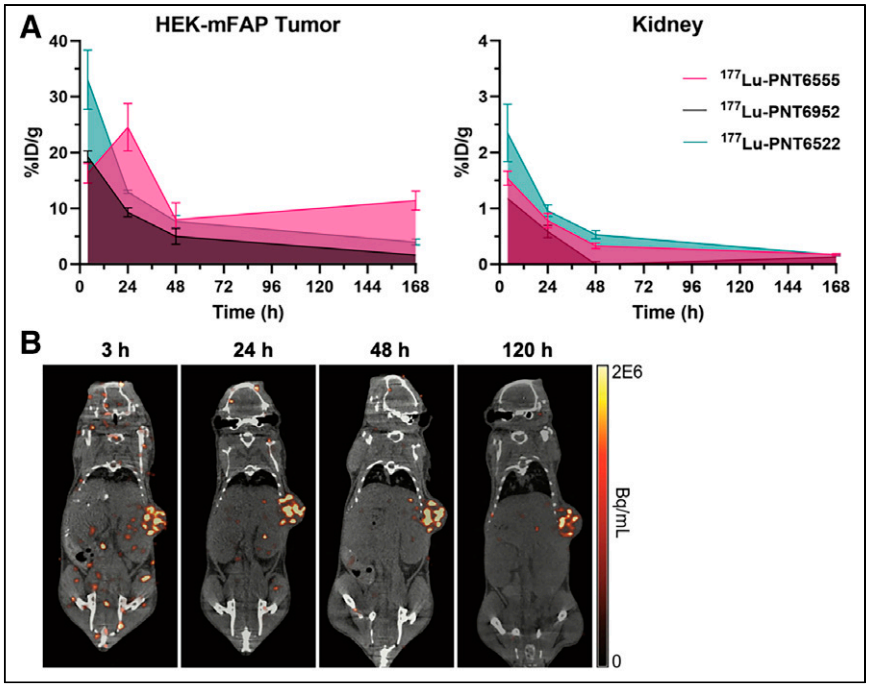

FIGURE 4. Biodistribution and SPECT imaging for ^{177}Lu-radioligands in mice bearing HEK-mFAP tumors administered doses of 6.8–7.8 MBq. (A) ^{177}Lu-PNT6555, ^{177}Lu-PNT6952, and ^{177}Lu-PNT6522 uptake in tumors and kidneys at 4 to 168 h after administration in animals bearing ~171-mm^3 tumors. Mean ± SEM %ID/g values are shown for 3 animals per tissue. Statistical analysis of AUC values indicated significantly greater accumulation in tumors of ^{177}Lu-PNT6555 than of ^{177}Lu-PNT6952 or ^{177}Lu-PNT6522 ($P < 0.0001$), and in kidneys there were no significant differences among AUC values for these radioligands. (B) Biodistribution of ^{177}Lu-PNT6555 determined by SPECT imaging 3, 24, 48, and 120 h after administration in representative animals (from groups of 3) bearing ~355-mm^3 tumors.

translatability of the results to humans. Although the FAP levels are artificially high, the HEK-mFAP model may, nevertheless, have utility because it brings the tumor/blood ratio of FAP closer to that of human cancer patients. Mice have greater circulating FAP levels than humans (*28*), and the tumor/blood ratio is a key determinant of tumor-selective targeting. Thus, the HEK-mFAP model could facilitate comparison of the FAP-targeting potential of various agents and might yield results that are predictive of human efficacy. A previous comparative study of the leading clinical candidates, FAP-2286 and FAPI-46, demonstrated the utility of HEK cells engineered to express human FAP in selection of clinical candidates (*24*), and the results provide feasible benchmarks for the new boronic acid derivatives. In humans, ^{68}Ga-FAPI-46-PET exhibited strong correlation with FAP tissue expression determined by immunohistochemistry (*33*), and ^{68}Ga-FAPI-46 PET/CT appeared to be equivalent to ^{18}F-FDG PET/CT for detection of malignant lesions in head and neck cancer (*34*). Moreover, first-in-human results for ^{177}Lu-FAP-2286 in advanced metastatic disease have demonstrated significant tumor uptake and longer tumor retention times compared with the earlier clinical candidates, FAPI-02 and FAPI-04 (*22*,*35*).

TABLE 3
Tissue Distribution After Intravenous Injection of ^{177}Lu-PNT6555, ^{177}Lu-PNT6952, and ^{177}Lu-PNT6522 in HEK-mFAP Xenograft Model

	AUC ((%ID/g)·h)			Tumor-to-normal tissue ratio		
Tissue	^{177}Lu-PNT6555	^{177}Lu-PNT6952	^{177}Lu-PNT6522	^{177}Lu-PNT6555	^{177}Lu-PNT6952	^{177}Lu-PNT6522
Blood	7.2	1.3	3.5	274.2	639.9	396.7
Heart	13.6	3.7	6.0	144.4	229.3	233.3
Lung	13.5	2.5	7.8	146.3	348.5	180.7
Liver	78.3	9.0	20.5	25.2	95.7	68.6
Spleen	46.7	12.1	24.0	42.2	71.1	58.7
Pancreas	16.0	3.1	6.1	122.9	280.2	231.1
Stomach	16.1	2.3	6.5	122.0	366.4	216.2
Small intestine	15.8	3.4	8.6	124.8	255.2	163.3
Kidney	67.1	32.6	92.9	29.3	26.3	15.2
Muscle	30.5	3.1	12.7	64.5	280.2	110.9
Bone (femur)	94.2	9.2	77.2	20.9	93.4	18.2
Skin	53.4	5.0	23.9	36.9	172.9	59.0
Brain	3.5	1.2	0.7	565.8	702.8	1,961.5
Tumor	1,969.0	857.4	1,408.4			

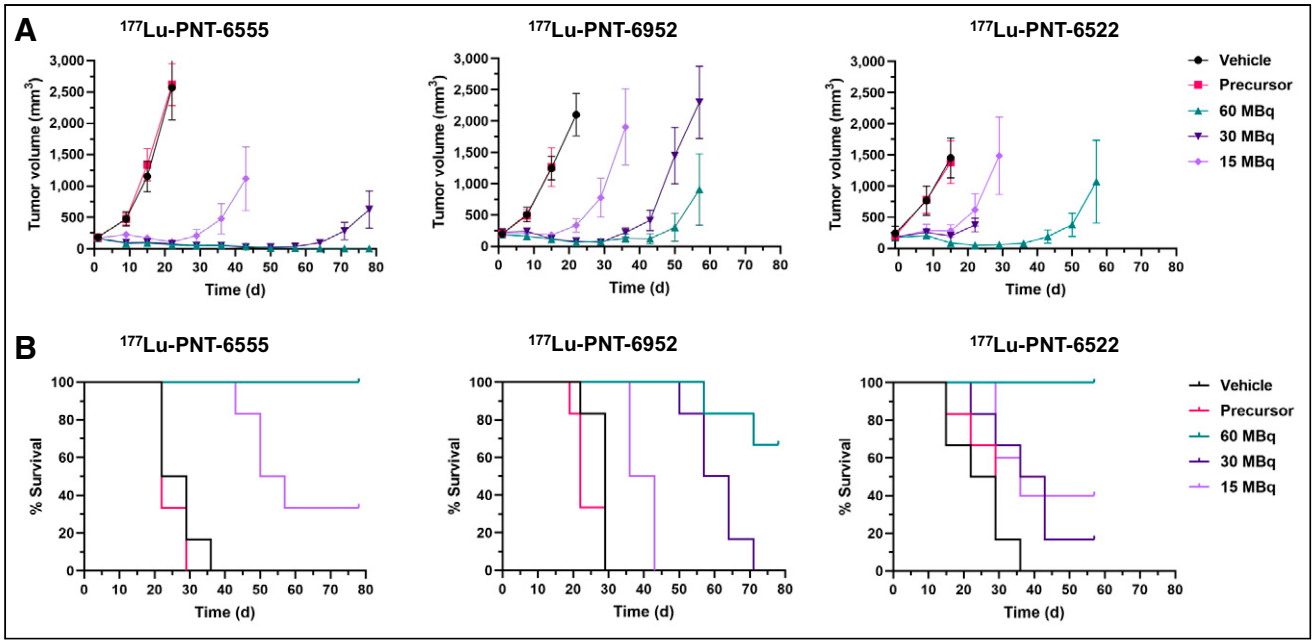

FIGURE 5. Antitumor activity of ^{177}Lu-PNT6555, ^{177}Lu-PNT6952, and ^{177}Lu-PNT6522 in mice bearing HEK-mFAP tumors. Animals bearing tumors that had grown to ~170–260 mm^3 were administered single intravenous injection of vehicle or test agent (6 animals/treatment) on day 1. (A) Tumor growth curves (mean ± SEM). (B) Animal survival curves. First day of tumor measurement was day 1, except in study of ^{177}Lu-PNT6522, for which first day of measurement was 1 day before treatment started. Compared with survival seen with vehicle treatment, survival was significantly increased by ^{177}Lu-PNT6555 and ^{177}Lu-PNT6952 at all 3 doses ($P \leq 0.001$) and by ^{177}Lu-PNT6522 at dose of 60 MBq ($P \leq 0.01$) but not at lower doses.

The biodistribution and PET imaging studies of ^{68}Ga-PNT6555 and ^{68}Ga-PNT6952 reported here demonstrated higher tumor specificity than ^{68}Ga-FAP-2286 or ^{68}Ga-FAPI-46. In addition, the tumor growth delay produced by ^{177}Lu-PNT6555 in the HEK-mFAP tumor model was greater than reported for ^{177}Lu-FAP-2286 and ^{177}Lu-FAPI-46 when the same single doses of 30 MBq were administered (*24*).

In the PANC-1 tumor model, FAP is expressed by stromal CAFs, and 30 MBq ^{177}Lu-FAPI-46 produced only an insignificant trend in tumor growth inhibition (*29*), whereas equivalent doses of ^{177}Lu-PNT6555, ^{177}Lu-PNT6952, and ^{177}Lu-PNT6522 produced much greater, statistically significant responses in the HEK-mFAP model. Similarly, 25 kBq ^{225}Ac-PNT6555 produced a significant HEK-mFAP tumor response, greatly exceeding the effect of ^{225}Ac-FAPI-46 in the PANC-1 model. These results raise an important question with respect to clinical translation. Are the efficacy results in the HEK-mFAP model artefactually exaggerated because of the unnaturally high and homogeneous overexpression of FAP in the HEK cells, or are the results in the PANC-1 model artificially suppressed by a low level of FAP expression in the tumor stroma and a circulating FAP level approximately 15-fold greater than in humans (*28*)? Compared with the tumor/blood FAP ratio in human cancer patients, the ratio in the PANC-1 mouse model might be lower, whereas the ratio in HEK-mFAP model is higher (S.E. Poplawski, PhD, unpublished data, 2010). As this ratio will be a key determinant of selective tumor targeting, it is unclear which model might more reliably predict

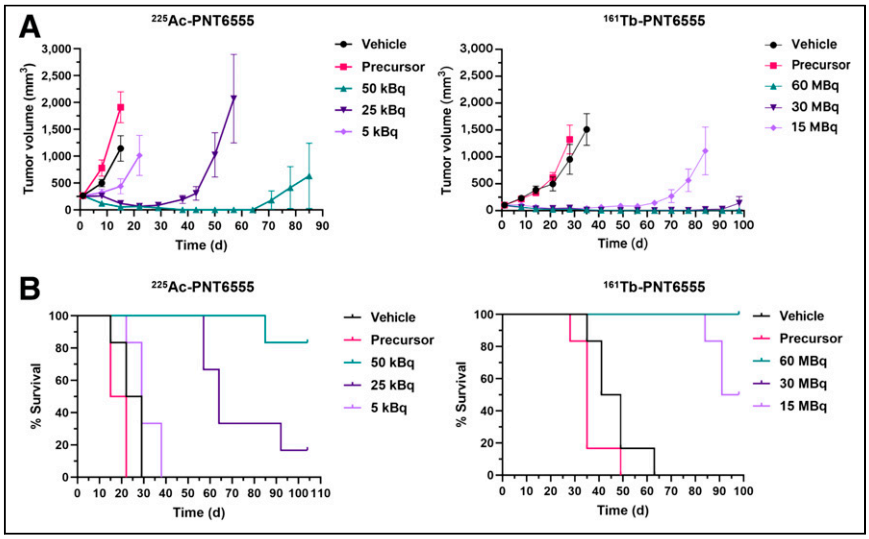

FIGURE 6. Antitumor activity of ^{225}Ac-PNT6555 and ^{161}Tb-PNT6555 in mice bearing HEK-mFAP tumors. Animals bearing tumors that had grown to ~250 mm^3 (^{225}Ac study) or ~100 mm^3 (^{161}Tb study) were administered single intravenous injection of vehicle or test agent (6 animals/treatment) on day 1. (A) Tumor growth curves (mean ± SEM tumor volume). (B) Animal survival curves. First day of tumor measurement was day 1. Compared with survival in precursor-treated animals, survival was significantly increased by ^{225}Ac-PNT6555 (50 and 25 kBq, $P \leq 0.001$; and 5 kBq, $P \leq 0.01$) and by ^{161}Tb-PNT6555 (60, 30, and 15 MBq; $P \leq 0.001$). At 60 and 30 MBq doses of ^{161}Tb-PNT6555, survival was 100%—curves fall on top of each other.

human efficacy. Better mouse models that naturally express greater levels of FAP in the tumor stroma while having less circulating FAP are definitely needed, but comparative results in humans and mice for clinical candidates may ultimately resolve this question.

Clinical translation of the PNT FAP ligands will require preclinical evaluation of possible longer-term adverse effects. In this regard, it is encouraging that tissues associated with known risks of renal and hematologic toxicity (*36*) did not show meaningful accumulation of ^{177}Lu-PNT6555. Any possible sink effect of the serum pool of FAP leading to off-target biodistribution, which would likely be exaggerated in mice, was not observed. In human cancer, FAP-positive CAFs provide critical support for tumor growth and metastasis by production and remodeling of extracellular matrix, release of growth factors and cytokines that directly stimulate tumor growth or promote angiogenesis, and suppression of tumor immunity (*37*). Targeting of FAP-positive stromal CAFs in human cancer, therefore, has potential for antitumor effects in addition to DNA damage in neoplastic cells, as would be expected in FAP-transfected tumor models (*38*). In FAP-positive human cancer there is the opportunity for antitumor effects by direct damage to FAP-expressing CAFs, and bystander effects on adjacent neoplastic cells by cross-fire irradiation and cytotoxic factors released by radiation damaged cells (*39*). Although cross-fire may be greater in larger tumors with β-particles, which have a range beyond a single cell layer, α-particles can afford greater cytotoxicity by producing more double-strand breaks in DNA and chromosomal aberrations (*40*). It appears desirable to optimize the type of radionuclide emission for the clinical stage of the cancer (*40*,*41*). If successfully translated to the clinic, the strong preclinical efficacy of PNT6555 chelated with ^{177}Lu, ^{161}Tb, or ^{225}Ac suggests that 3099-based FAP ligands might offer the flexibility required to deliver α- or β-emitting radiometals to the tumor bed, either concomitantly or sequentially.

CONCLUSION

The preclinical results support the advancement of PNT6555 to the "FAPi Radioligand Open-Label, Phase 1 Study to Evaluate Safety, Tolerability and Dosimetry of [Lu-177]-PNT6555: A Dose Escalation Study for Treatment of Patients with Select Solid Tumors (FRONTIER)" (ClinicalTrials.gov identifier NCT05432193).

DISCLOSURE

This work was funded by POINT Biopharma Global Inc. Sarah Poplawski, Shuang Pan, Wengen Wu, Yuxin Liu, Barry Jones, Jack Lai, and William Bachovchin are employees of Tufts University and collaborate with POINT Biopharma Global Inc. under a sponsored research agreement. William Bachovchin consults for POINT Biopharma Global Inc. and holds stock or stock options in POINT Biopharma Global Inc. Robin Hallett, Mark Dornan, Kyle Novakowski, Valerie Hergott, Albert Felten, and Joe McCann are employees and stockholders of POINT Biopharma Global Inc. Quang-De Nguyen previously consulted for POINT Biopharma Global Inc. and collaborates with POINT Biopharma Global Inc. under a fee-for-service agreement. Anthony Belanger and Shin Hye Ahn collaborate with POINT Biopharma Global Inc. under a fee-for-service agreement.

ACKNOWLEDGMENT

The ^{225}Ac used in this research was supplied by the U.S. Department of Energy Isotope Program managed by the Office of Isotope R&D and Production.

KEY POINTS

QUESTION: Are boronic acid–based DOTA-FAPIs effective as PET tracers and anticancer agents when chelated with diagnostic and therapeutic radiometals?

PERTINENT FINDINGS: Boronic acid–based DOTA-FAPIs are potent, selective inhibitors of soluble and membrane-associated forms of FAP. In a FAP-positive tumor model, the ^{68}Ga-chelates of PNT6555 and PNT6952 exhibited appropriate properties for PET imaging, and the ^{177}Lu-chelates of PNT6555, PNT6952, and PNT6522 produced strong anticancer effects, with PNT6555 exhibiting the most potent antitumor activity when chelated with ^{177}Lu and similar activity when chelated with ^{225}Ac or ^{161}Tb, suggesting versatility in therapeutic applications.

IMPLICATIONS FOR PATIENT CARE: PNT6555- and 3099-based analogs provide feasible alternatives to quinoline-based DOTA-FAPIs, and the preclinical results support their translation to the clinic for theranostic applications in oncology.

REFERENCES

1. Waumans Y, Baerts L, Kehoe K, Lambeir AM, De Meester I. The dipeptidyl peptidase family, prolyl oligopeptidase, and prolyl carboxypeptidase in the immune system and inflammatory disease, including atherosclerosis. *Front Immunol.* 2015;6:387.
2. Busek P, Malik R, Sedo A. Dipeptidyl peptidase IV activity and/or structure homologues (DASH) and their substrates in cancer. *Int J Biochem Cell Biol.* 2004;36:408–421.
3. Rosenblum JS, Kozarich JW. Prolyl peptidases: a serine protease subfamily with high potential for drug discovery. *Curr Opin Chem Biol.* 2003;7:496–504.
4. Scanlan MJ, Raj BK, Calvo B, et al. Molecular cloning of fibroblast activation protein alpha, a member of the serine protease family selectively expressed in stromal fibroblasts of epithelial cancers. *Proc Natl Acad Sci USA.* 1994;91:5657–5661.
5. Lee KN, Jackson KW, Christiansen VJ, Lee CS, Chun JG, McKee PA. Antiplasmin-cleaving enzyme is a soluble form of fibroblast activation protein. *Blood.* 2006;107:1397–1404.
6. Park JE, Lenter MC, Zimmermann RN, Garin-Chesa P, Old LJ, Rettig WJ. Fibroblast activation protein, a dual specificity serine protease expressed in reactive human tumor stromal fibroblasts. *J Biol Chem.* 1999;274:36505–36512.
7. Nurmik M, Ullmann P, Rodriguez F, Haan S, Letellier E. In search of definitions: cancer-associated fibroblasts and their markers. *Int J Cancer.* 2020;146:895–905.
8. Dolznig H, Schweifer N, Puri C, et al. Characterization of cancer stroma markers: in silico analysis of an mRNA expression database for fibroblast activation protein and endosialin. *Cancer Immun.* 2005;5:10.
9. Hamson EJ, Keane FM, Tholen S, Schilling O, Gorrell MD. Understanding fibroblast activation protein (FAP): substrates, activities, expression and targeting for cancer therapy. *Proteomics Clin Appl.* 2014;8:454–463.
10. Liu R, Li H, Liu L, Yu J, Ren X. Fibroblast activation protein: a potential therapeutic target in cancer. *Cancer Biol Ther.* 2012;13:123–129.
11. Acharya PS, Zukas A, Chandan V, Katzenstein AL, Pure E. Fibroblast activation protein: a serine protease expressed at the remodeling interface in idiopathic pulmonary fibrosis. *Hum Pathol.* 2006;37:352–360.
12. Bauer S, Jendro MC, Wadle A, et al. Fibroblast activation protein is expressed by rheumatoid myofibroblast-like synoviocytes. *Arthritis Res Ther.* 2006;8:R171.
13. Garin-Chesa P, Old LJ, Rettig WJ. Cell surface glycoprotein of reactive stromal fibroblasts as a potential antibody target in human epithelial cancers. *Proc Natl Acad Sci USA.* 1990;87:7235–7239.
14. Busek P, Mateu R, Zubal M, Kotackova L, Sedo A. Targeting fibroblast activation protein in cancer: prospects and caveats. *Front Biosci (Landmark Ed).* 2018;23:1933–1968.
15. Alcocer-Ávila ME, Ferreira A, Quinto MA, Morgat C, Hindie E, Champion C. Radiation doses from ^{161}Tb and ^{177}Lu in single tumour cells and micrometastases. *EJNMMI Phys.* 2020;7:33.
16. Calais J. FAP: the next billion dollar nuclear theranostics target? *J Nucl Med.* 2020;61:163–165.
17. Moller DE. New drug targets for type 2 diabetes and the metabolic syndrome. *Nature.* 2001;414:821–827.
18. D'Agostino G, Kim JD, Liu ZW, et al. Prolyl endopeptidase-deficient mice have reduced synaptic spine density in the CA1 region of the hippocampus, impaired LTP, and spatial learning and memory. *Cereb Cortex.* 2013;23:2007–2014.

19. Ryabtsova O, Jansen K, Van Goethem S, et al. Acylated Gly-(2-cyano)pyrrolidines as inhibitors of fibroblast activation protein (FAP) and the issue of FAP/prolyl oligopeptidase (PREP)-selectivity. *Bioorg Med Chem Lett.* 2012;22:3412–3417.
20. Jansen K, Heirbaut L, Cheng JD, et al. Selective inhibitors of fibroblast activation protein (FAP) with a (4-Quinolinoyl)-glycyl-2-cyanopyrrolidine scaffold. *ACS Med Chem Lett.* 2013;4:491–496.
21. Jansen K, Heirbaut L, Verkerk R, et al. Extended structure-activity relationship and pharmacokinetic investigation of (4-quinolinoyl)glycyl-2-cyanopyrrolidine inhibitors of fibroblast activation protein (FAP). *J Med Chem.* 2014;57:3053–3074.
22. Lindner T, Loktev A, Altmann A, et al. Development of quinoline-based theranostic ligands for the targeting of fibroblast activation protein. *J Nucl Med.* 2018;59: 1415–1422.
23. Zboralski D, Hoehne A, Bredenbeck A, et al. Comparative biodistribution and radiotherapeutic efficacy of the fibroblast activation protein (FAP)–targeting agents FAP-2286 and FAPI-46. In: *Proceedings of the Annual Meeting of the American Association of Cancer Research.* Philadelphia, PA: AACR; 2022. Abstract 3317/15.
24. Zboralski D, Hoehne A, Bredenbeck A, et al. Preclinical evaluation of FAP-2286 for fibroblast activation protein targeted radionuclide imaging and therapy. *Eur J Nucl Med Mol Imaging.* 2022;49:3651–3667.
25. Poplawski SE, Lai JH, Li Y, et al. Identification of selective and potent inhibitors of fibroblast activation protein and prolyl oligopeptidase. *J Med Chem.* 2013;56: 3467–3477.
26. Bachovchin WW, Lai H-S, Wu W. FAP-targeted pharmaceuticals and imaging agents, and uses related thereto. WO patent 11707539. July 25, 2023.
27. Cheng JD, Dunbrack RL Jr, Valianou M, Rogatko A, Alpaugh RK, Weiner LM. Promotion of tumor growth by murine fibroblast activation protein, a serine protease, in an animal model. *Cancer Res.* 2002;62:4767–4772.
28. Keane FM, Yao TW, Seelk S, et al. Quantitation of fibroblast activation protein (FAP)-specific protease activity in mouse, baboon and human fluids and organs. *FEBS Open Bio.* 2013;4:43–54.
29. Liu Y, Watabe T, Kaneda-Nakashima K, et al. Fibroblast activation protein targeted therapy using [^{177}Lu]FAPI-46 compared with [^{225}Ac]FAPI-46 in a pancreatic cancer model. *Eur J Nucl Med Mol Imaging.* 2022;49:871–880.
30. Müller C, Reber J, Haller S, et al. Direct in vitro and in vivo comparison of ^{161}Tb and ^{177}Lu using a tumour-targeting folate conjugate. *Eur J Nucl Med Mol Imaging.* 2014;41:476–485.
31. Grünberg J, Lindenblatt D, Dorrer H, et al. Anti-L1CAM radioimmunotherapy is more effective with the radiolanthanide terbium-161 compared to lutetium-177 in an ovarian cancer model. *Eur J Nucl Med Mol Imaging.* 2014;41:1907–1915.
32. Lindeman SD, Mukkamala R, Horner A, et al. Fibroblast activation protein–targeted radioligand therapy for treatment of solid tumors. *J Nucl Med.* 2023; 64:759–766.
33. Mona CE, Benz MR, Hikmat F, et al. Correlation of ^{68}Ga-FAPi-46 PET biodistribution with FAP expression by immunohistochemistry in patients with solid cancers: interim analysis of a prospective translational exploratory study. *J Nucl Med.* 2022;63:1021–1026.
34. Wegen S, van Heek L, Linde P, et al. Head-to-head comparison of [^{68}Ga]Ga-FAPI-46-PET/CT and [^{18}F]F-FDG-PET/CT for radiotherapy planning in head and neck cancer. *Mol Imaging Biol.* 2022;24:986–994.
35. Baum RP, Schuchardt C, Singh A, et al. Feasibility, biodistribution, and preliminary dosimetry in peptide-targeted radionuclide therapy of diverse adenocarcinomas using ^{177}Lu-FAP-2286: first-in-humans results. *J Nucl Med.* 2022;63:415–423.
36. Camus B, Cottereau AS, Palmieri LJ, et al. Indications of peptide receptor radionuclide therapy (PRRT) in gastroenteropancreatic and pulmonary neuroendocrine tumors: an updated review. *J Clin Med.* 2021;10:1267.
37. Sahai E, Astsaturov I, Cukierman E, et al. A framework for advancing our understanding of cancer-associated fibroblasts. *Nat Rev Cancer.* 2020;20:174–186.
38. O'Neill E, Kersemans V, Allen PD, et al. Imaging DNA damage repair in vivo after ^{177}Lu-DOTATATE therapy. *J Nucl Med.* 2020;61:743–750.
39. Xue LY, Butler NJ, Makrigiorgos GM, Adelstein SJ, Kassis AI. Bystander effect produced by radiolabeled tumor cells in vivo. *Proc Natl Acad Sci USA.* 2002;99: 13765–13770.
40. Haberkorn U, Giesel F, Morgenstern A, Kratochwil C. The future of radioligand therapy: alpha, beta, or both? *J Nucl Med.* 2017;58:1017–1018.
41. Feuerecker B, Tauber R, Knorr K, et al. Activity and adverse events of actinium-225-PSMA-617 in advanced metastatic castration-resistant prostate cancer after failure of lutetium-177-PSMA. *Eur Urol.* 2021;79:343–350.